Z. Phys. C - Particles and Fields 55, 619–626 (1992)

Zeitschrift für Physik C Particles and Fields

Measuring the $WW\gamma$ vertex in the process $ep \to \gamma\nu X$

Stephen Godfrey

Ottawa Carleton Institute for Physics, Department of Physics, Carleton University, K1S 5B6 Ottawa, Canada

Received 30 July 1991; final version 21 April 1992

Abstract. We present a detailed analysis of the process $ep \to \gamma\nu X$ as a means of studying the gauge structure of the $WW\gamma$ vertex. We find that the differential cross section of high p_T photons offers a sensitive measure of anomalous $WW\gamma$ couplings. At HERA ($\sqrt{s} = 314$ GeV), after several years of running, the $WW\gamma$ vertex can be measured to $\delta\kappa_\gamma \simeq {}^{+2.9}_{-2.0}$ and $\delta\lambda_\gamma \simeq {}^{+3.0}_{-2.5}$ (95% C.L.) which offers an improvement over existing constraints from direct measurements using associated $W\gamma$ production in $\bar{p}p$ collisions but is less sensitive than the competing process at HERA, $ep \to eWX$. For a higher energy ep collider, LEP-LHC ($\sqrt{s} = 1.3$ TeV), the $WW\gamma$ vertex can be measured to $\delta\kappa_\gamma \simeq \pm 0.4$ and $\delta\lambda_\gamma \simeq \pm 0.1$ at 95% C.L. which is more sensitive to λ_γ than the process $e^+e^- \to W^+W^-$ at the LEP200 e^+e^- collider and is comparable to the LEP200 sensitivity to κ_γ. These values are also roughly comparable to the competing process $ep \to eWX$ at LEP-LHC and to what is expected from associated γW production at the LHC and SSC for κ_γ but they are about half as sensitive to λ_γ as the LHC and SSC.

1 Introduction

Although the Standard Model of the electroweak interactions [1] is consistent with all experimental measurements [2] there is a growing consensus that it is an effective low energy limit of a deeper, more fundamental theory [3]. One probe for physics beyond the standard model is precision measurements of the standard model [4]. The fermion–gauge boson couplings of the theory are being tested to ever increasing precision at the LEP e^+e^- collider [5] and elsewhere both at tree level and via higher loop radiative corrections [4]. However, the gauge boson couplings, and hence the non-Abelian nature of the standard model, have yet to be subjected to rigorous direct experimental tests. Measuring the $WW\gamma$ and WWZ^0 couplings is one of the primary objectives of the LEP200 e^+e^- collider ($\sqrt{s} = 200$ GeV) which will study W-boson pair production in the process $e^+e^- \to W^+W^-$ [6–9]. A drawback of this process is that both the $WW\gamma$ and WWZ^0 vertices contribute roughly equally so that only a linear combination of the two will effectively be measured. It is therefore important that independent measurements of these couplings be made which will complement the LEP200 analysis.

In the near future, possibilities for measuring the trilinear gauge boson vertex are associative $W\gamma$ production at hadron colliders [9–12] and single W production in ep colliders [13–16]. These have been examined elsewhere. In this paper we consider the hitherto ignored process $ep \to \gamma\nu X$ [17] to see whether the $WW\gamma$ vertex can be measured with sufficient precision to be competitive with other processes.

The ep colliders we consider [18] are the HERA ep collider at DESY [19], 30 GeV electrons on 820 GeV protons, $\sqrt{s} \simeq 314$ GeV, with luminosity of $1.5 \times 10^{31}\,\mathrm{cm}^{-1}\,\mathrm{s}^{-1}$, yielding $\sim 200\,\mathrm{pb}^{-1}$/year, a hypothetical HERA upgrade with 35 GeV electrons on 1200 GeV protons, $\sqrt{s} \simeq 410$ GeV, (HERA′ with the same luminosity as HERA), and for ep colliders in the LEP tunnel [20] with 50 GeV electrons on 8 TeV protons, $\sqrt{s} \simeq 1.3$ TeV, with $\mathscr{L} = 10^{32}\,\mathrm{cm}^{-1}\,\mathrm{s}^{-1}$ yielding $1000\,\mathrm{pb}^{-1}$/year, LEP-LHC, and 100 GeV electrons on 8 TeV protons, $\sqrt{s} \simeq 1.8$ TeV, with $\mathscr{L} = 10^{31}\,\mathrm{cm}^{-1}\,\mathrm{s}^{-1}$ yielding $100\,\mathrm{pb}^{-1}$/year, LEP2-LHC. We find that this process's sensitivity to anomalous couplings is less than half as sensitive as the single W production process $ep \to eWX$ at HERA and is roughly comparable to the single W production process at a LEP × LHC ep collider.

2 The trilinear vector boson couplings

Within the Standard Model the $WW\gamma$ vertex is uniquely determined by $SU(2)_L \times U(1)$ gauge invariance so that a precise measurement of the vertex poses a severe test of the gauge structure of the theory. The most general $WW\gamma$ vertex, consistent with Lorentz invariance, can be parametrized in terms of seven form factors when the

W bosons couple to essentially massless fermions which effectively results in $\partial_\mu W^\mu = 0$ [6, 21]. For on shell photons electromagnetic gauge invariance further restricts the tensor structure of the $WW\gamma$ vertex to allow only four free parameters, two of which violate CP invariance. Measurement of the neutron electron dipole moment constrains the two CP violating parameters, $\tilde{\kappa}_\gamma$ and $\tilde{\lambda}_\gamma$, to values smaller than gives rise to observable effects in the process we are considering; $|\tilde{\kappa}_\gamma|, |\tilde{\lambda}_\gamma| < \mathcal{O}(10^{-4})$ [22, 23]. Therefore, the most general Lorentz and CP invariant vertex compatible with electromagnetic gauge invariance is commonly parametrized as [6, 21]:

$$\mathcal{L}WW\gamma = -ie\left\{(W^\dagger_{\mu\nu} W^\mu A^\nu - W^\dagger_\mu A_\nu W^{\mu\nu}) + \kappa_\gamma W^\dagger_\mu W_\nu F^{\mu\nu} + \frac{\lambda_\gamma}{M_W^2} W^\dagger_{\lambda\mu} W^\mu_\nu F^{\nu\lambda}\right\}, \quad (1)$$

where A^μ and W^μ are the photon and W^- fields, $W_{\mu\nu} = \partial_\mu W_\nu - \partial_\nu W_\mu$ and $F_{\mu\nu} = \partial_\mu A_\nu - \partial_\nu A_\mu$ denote the W and photon field strength tensors, and M_W is the W boson mass. Higher dimension operators correspond to momentum dependence in the form factors. The first term, referred to as the minimal coupling term, simply reflects the charge of the W. The Feynman rule for the $WW\gamma$ vertex resulting from (1) is given by:

$$\begin{aligned} ie\{&g_{\alpha\beta}[(1-\tilde{\lambda}k_-\cdot q)k_{+\mu} - (1-\tilde{\lambda}k_+\cdot q)k_{-\mu}] \\ &- g_{\alpha\mu}[(1-\tilde{\lambda}k_-\cdot q)k_{+\beta} - (\kappa-\tilde{\lambda}k_+\cdot k_-)q_\beta] \\ &- g_{\beta\mu}[(\kappa-\tilde{\lambda}k_-\cdot k_+)q_\alpha - (1-\tilde{\lambda}k_+\cdot q)k_{-\alpha}] \\ &+ \tilde{\lambda}(k_{+\mu}k_{-\alpha}q_\beta - k_{-\mu}q_\alpha k_{+\beta})\}, \end{aligned} \quad (2)$$

with the notation and conventions given in Fig. 1 and where $\tilde{\lambda} = \lambda/M_W^2$. The free parameters κ_γ and λ_γ are related to the anomalous magnetic dipole moment μ_W and the electric quadrupole moment Q_W of the W by

$$\mu_W = \frac{e}{2M_W}(1+\kappa_\gamma+\lambda_\gamma), \quad Q_W = \frac{e}{M_W^2}(\lambda_\gamma - \kappa_\gamma). \quad (3)$$

At tree level the Standard Model predicts $\kappa_\gamma = 1$ and $\lambda_\gamma = 0$.

Deviations from the Standard Model lead to amplitudes which grow with energy and therefore violate unitarity at high energy [24]. To avoid violation of the unitarity bound, one should include a momentum dependence in the form factors which vanishes when the square of the four momentum of one of the vector bosons becomes large, which might take the form $(1+s/\Lambda^2)^{-n}$ where Λ represents the scale at which new physics becomes important and n is chosen as the minimum value compatible with unitarity [6]. Since one expects that the scale of new physics is of the order of 1 TeV, for the energies we are considering it is not unreasonable to ignore the momentum dependence of the form factors.

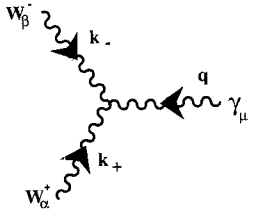

Fig. 1. The Feynman Diagram for the $WW\gamma$ corresponding to the Feynman rule of (1)

3 Calculations and results

The Feynman diagrams contributing to the parton level cross section for $e^- p \to \gamma \nu X$ are given in Fig. 2. The $WW\gamma$ vertex we are interested in contributes via diagram 2a. To preserve electromagnetic gauge invariance and to properly take into account the possible background processes our calculation includes all the parton level diagrams of Fig. 2 for arbitrary values of κ_γ and λ_γ. To evaluate the cross section and distributions we used the CALKUL helicity amplitude technique [25] to obtain expressions for the matrix elements. The CALKUL method is summarized in the Appendix where we also write down the helicity amplitudes corresponding to the Feynman diagrams of Fig. 2. Monte Carlo integration techniques are then used to perform the phase space integrals [26]. For the structure functions we used Duke–Owens set 1 [27] with the scale, Q^2, given by the four momentum transfer of the scattered quark, $Q^2 = -(p_q - p_{q'})^2$ where $p_q(p_{q'})$ is the four momentum of the initial (final) state quarks. With our cuts, the constraint $Q^2 > 4$ GeV^2 is automatically fulfilled. We included u and c quarks and d and s antiquarks in our

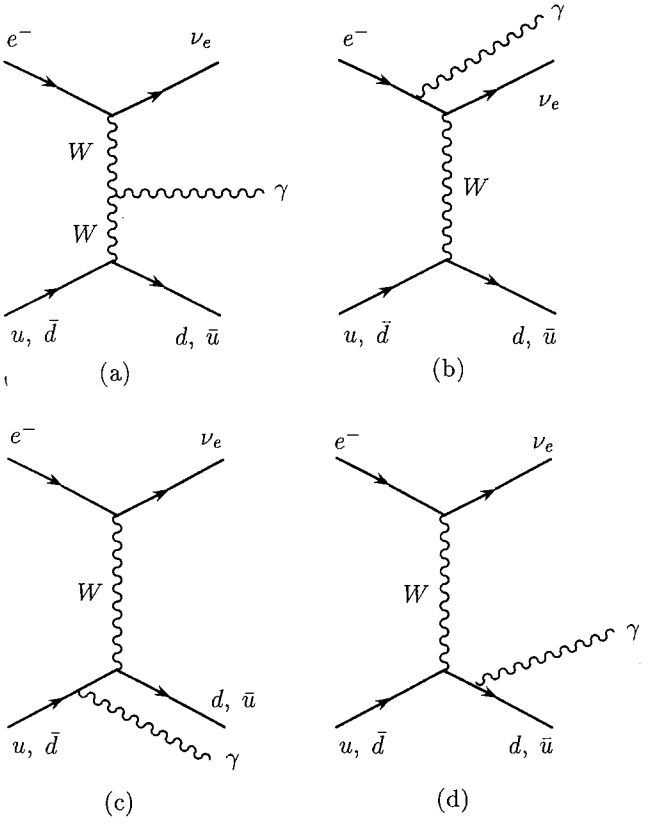

Fig. 2a–d. Feynman diagrams for the parton level processes contributing to $ep \to \nu\gamma X$

calculations. Thus the matrix element squared is given by

$$\sum_{q=u,c}\left[\left|\sum_{i=a,b,c,d} M_L^i(eq\to\nu\gamma q')\right|^2 + \left|\sum_{i=a,b,c,d} M_R^i(eq\to\nu\gamma q')\right|^2\right] f_{q/P}(x,Q^2) + \sum_{\bar{q}=\bar{d},\bar{s}}\left[\left|\sum_{i=\bar{a},\bar{b},\bar{c},\bar{d}} M_L^i(e\bar{q}\to\nu\gamma\bar{q}')\right|^2 + \left|\sum_{i=\bar{a},\bar{b},\bar{c},\bar{d}} M_R^i(e\bar{q}\to\nu\gamma\bar{q}')\right|^2\right] f_{\bar{q}/P}(x,Q^2), \quad (4)$$

where the subscript, L or R is the helicity of the outgoing photon, the quark (antiquark) momentum, $p_q(p_{\bar{q}})$ is the fraction x of the proton momentum, and the helicity amplitudes are given in the Appendix. For our numerical results we take $\alpha=1/137$, $M_W=80$ GeV, $\Gamma_W=2.0$ GeV, and $\sin^2\theta_W=0.23$.

The signal consists of a high transverse momentum (p_T) photon, large missing transverse momentum ($\not{p}_T$) due to the neutrino and a jet due to the scattered quark from the beam proton. We do not include fragmentation and hadronization effects and identify the hadron jet momentum with that of the scattered quark. Therefore, the signal we are considering is:

$$e^-p\to\gamma+\not{p}_T+\text{jet}. \quad (5)$$

We require that for the observed photon and jet $7.5^\circ<\theta_{\gamma,\text{jet}}<170^\circ$ with respect to the proton direction which is appropriate to the ZEUS detector [18, 28] at HERA.* The angular cut also has the benefit of reducing the bremstrahlung photons collinear to the incoming fermions which dominate the cross section and obscure the diagram we wish to study. In order to roughly simulate detector response we impose additional cuts on $p_{T\gamma}$, $p_{T\text{jet}}$, and $\not{p}_T$. The signal at low p_T is insensitive to the $WW\gamma$ vertex so no sensitivity is lost by imposing these cuts. Because the low $p_{T\gamma}$ region is insensitive to the $WW\gamma$ vertex it will be useful in providing a normalization of the cross sections. In addition, we impose an isolation cut on the photon and jet of

$$R=[(\Delta\eta)^2+(\Delta\phi)^2]^{1/2}>0.5,$$

where η is the rapidity and ϕ is the azimuthal angle. This eliminates the problem of misidentifying π^0's in the hadron jet as photons and has the additional benefit of eliminating uninteresting contributions from final state bremstrahlung. With the cuts $p_{T\gamma}$, $p_{T\text{jet}}>5$ GeV, and $\not{p}_T>10$ GeV but no angular cuts, we show in Fig. 3 the $e^-p\to\gamma+\not{p}_T+$jet cross section, calculated in the center of mass frame, as a function of $\sqrt{s}$ for several values of anomalous couplings. With these cuts the Standard Model values for $\sigma(e^-p\to\nu_e\gamma X)$ are $\sim$0.74 pb for HERA, $\sim$1.2 pb for HERA′, $\sim$5.5 pb for LEP-LHC, and $\sim$8.3 pb for LEP2-LHC. If we calculate the cross section in the respective lab frames and include the angular cuts we find $\sigma\sim0.64$ pb and ~0.98 pb for HERA and HERA′ respectively. For LEP-LHC and LEP2-LHC we use $p_{T\gamma}$, $p_{T\text{jet}}>10$ GeV, and $\not{p}_T>20$ GeV and obtain $\sigma\sim1.6$ pb and ~2.8 pb respectively.

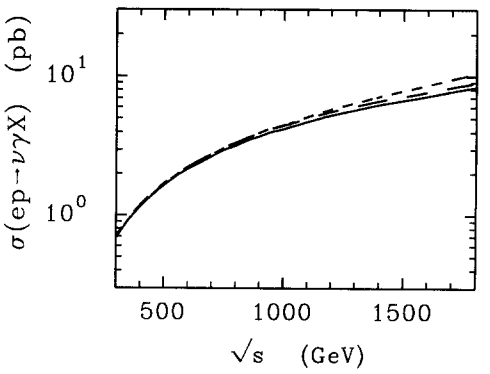

Fig. 3. The cross section $\sigma(ep\to\nu\gamma X)$ as a function of the center of mass energy with the kinematic cuts described in the text. The solid line is for the Standard Model, the long dashed line for $\kappa_\gamma=0$ and $\lambda_\gamma=0$, and the short dashed line for $\kappa_\gamma=1$ and $\lambda_\gamma=1$

The $p_{T\gamma}$ distributions for HERA and LEP-LHC, for several values of κ_γ and λ_γ, are shown in Fig. 4a and b respectively. These distributions were evaluated in the laboratory frame with the cuts $p_{T\gamma}$, $p_{T\text{jet}}>5$ GeV, $\not{p}_T>10$ GeV for HERA (and HERA′ in what follows) and $p_{T\gamma}$, $p_{T\text{jet}}>10$ GeV, $\not{p}_T>20$ GeV for LEP-LHC (and LEP200-LHC in what follows) to roughly simulate detector response. We used the angular cuts and isolation cut on the photon and jet described in the previous paragraph. Anomalous $WW\gamma$ couplings lead to an enhanced event rate at large values of the photon momentum. Terms proportional to λ_γ grow much faster than κ_γ terms with $p_{T\gamma}$, p^2/M_W^2 vs $\sqrt{p^2}/M_W$, with p the 4-momentum flowing through the legs in the vertex, which is apparent at large $p_{T\gamma}$. An advantage of $ep\to\nu\gamma X$ over $ep\to eWX$ is that one doesn't have the problem of misinterpreting variations κ_γ as normalization errors that one has to deal with in single W production in ep [14–16]. At small values of $p_{T\gamma}$, anomalous values of κ_γ produce larger deviations from the Standard Model than equal values of λ_γ while at large $p_{T\gamma}$ the cross section is far more sensitive to variations in λ_γ than κ_γ. Because the cross section is much smaller at large values of $p_{T\gamma}$, at HERA the reaction has roughly the same sensitivity to anomalous values of λ_γ and κ_γ. However, if deviations were observed, the shape of the $p_{T\gamma}$ distribution would be important for unravelling the nature of the anomalous coupling. In any case it would take a relatively large deviation in κ_γ or λ_γ to produce a measurable effect in $ep\to\nu\gamma X$ at HERA. In contrast, since LEP-LHC probes a higher energy scale, it turns out that the reaction is more sensitive to λ_γ than κ_γ although both can be measured to considerably higher accuracy than at HERA.

To quantify the sensitivity of the $p_{T\gamma}$ spectrum to anomalous $WW\gamma$ couplings we consider the values of κ_γ and λ_γ that give rise to deviations from the Standard Model at the 68%, 90%, and 95% confidence level. To

* Strictly speaking this corresponds to the central tracking region. The electromagnetic calorimetry and hadron calorimetry gives slightly larger angular coverage but this will not affect our results and conclusions [18, 28]

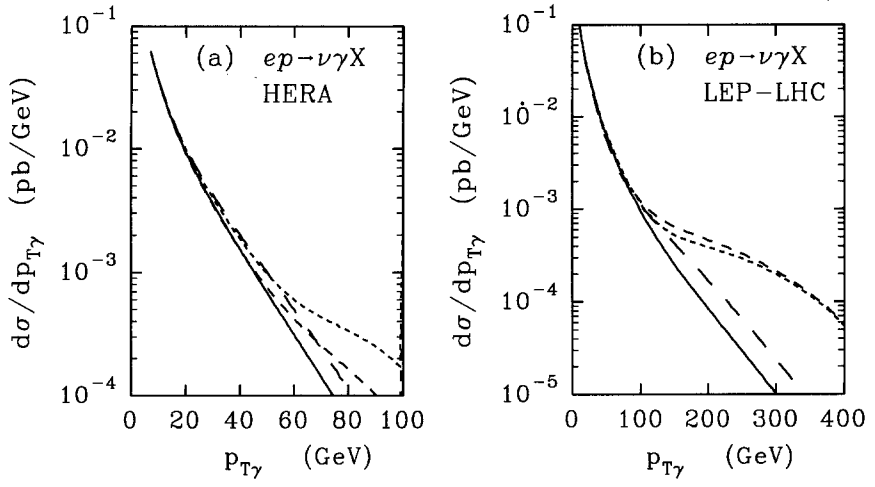

Fig. 4a, b. The transverse momentum distribution for the photon in the process $ep \to \nu\gamma X$. **a** For HERA, the solid line represents the Standard Model, the long dashed line is for $\kappa_\gamma = 2$ and $\lambda_\gamma = 0$, the medium dashed line is for $\kappa_\gamma = 1$, and $\lambda_\gamma = -2$, and the short dashed line is for $\lambda_\gamma = 4$ and $\kappa_\gamma = 1$. **b** For LEP-LHC the solid line represents the Standard Model, the long dashed line is for $\kappa_\gamma = 2$ and $\lambda_\gamma = 0$, the medium dashed line is for $\kappa_\gamma = 1$ and $\lambda_\gamma = -0.5$, and the short dashed line is for $\lambda_\gamma = +0.5$ and $\kappa_\gamma = 1$. Small irregularities in the curves are due to the statistical nature of the Monte Carlo integration technique

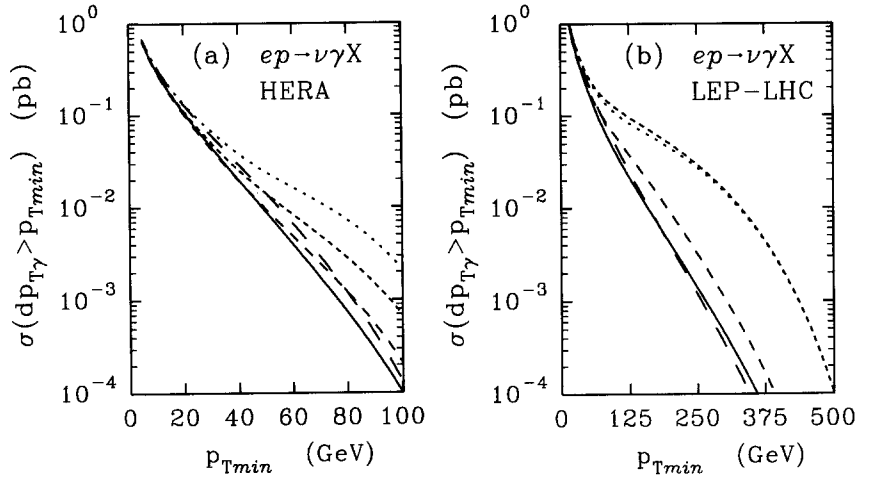

Fig. 5a, b. The total cross section for $p_{T\gamma} > p_{T\min}$ versus $p_{T\min}$ for $ep \to \nu\gamma X$. **a** For HERA, the solid line represents the Standard Model, the long dashed line is for $\kappa_\gamma = -1$ and $\lambda_\gamma = 0$, the medium dashed line is for $\kappa_\gamma = 2$ and $\lambda_\gamma = 0$, the short dashed line is for $\kappa_\gamma = 0$ and $\lambda_\gamma = -2$, and the dotted line is for $\lambda_\gamma = 4$ and $\kappa_\gamma = 1$. **b** For LEP-LHC the solid line represents the Standard Model, the long dashed line is for $\kappa_\gamma = 0$ and $\lambda_\gamma = 0$, the medium dashed line is for $\kappa_\gamma = 2$ and $\lambda_\gamma = 0$, the short dashed line is for $\kappa_\gamma = 1$ and $\lambda_\gamma = -0.5$, and the dotted line is for $\lambda_\gamma = +0.5$ and $\kappa_\gamma = 1$

find these bounds the cross section measurement and several kinematic distributions were considered with the most sensitive measurement being the transverse momentum distribution of the photon. We examined several different strategies to quantify the deviations of the $p_{T\gamma}$ distributions between the Standard Model and different values of κ_γ and λ_γ. For example, one approach was to divide the $p_{T\gamma}$ distribution into bins and calculate the χ^2 with respect to the Standard Model. Another approach was to consider the statistical significance of deviations using the integrated cross section while varying $p_{T\gamma}$(min), the lower limit of integration. In Fig. 5 we show the integrated cross section above a minimum transverse momentum cutoff $p_{T\min}$ for the photon for HERA and LEP-LHC. Since dividing the $p_{T\gamma}$ distribution into bins increased the number of degrees of freedom in the fit, using the integrated cross section with an optimized $p_{T\gamma}$(min) resulted in the largest statistical significance and hence the most sensitivity to anomalous couplings. However, if discrepancies were observed studying the $p_{T\gamma}$ distribution via binning would be crucial to understanding whether the discrepancy is due to deviations in κ_γ or λ_γ.

In Fig. 6 we show the values of κ_γ and λ_γ that would produce deviations at 68%, 90%, and 95% C.L. obtained by dividing $p_{T\gamma}$ into 3 bins. For HERA the $p_{T\gamma}$ bins used were 20–40, 40–60 and >60 GeV; for HERA′ 20–50, 50–80, and >80 GeV; for LEP-LHC 25–100, 100–175, and >175 GeV; and for LEP2-LHC 30–100, 100–175, >175 GeV. The results for the HERA and HERA′ colliders, assuming 1000 pb^{-1} integrated luminosity which represents several years of running, are shown in Fig. 6a and b and for the LEP-LHC and LEP2-LHC colliders assuming 5000 pb^{-1} and 500 pb^{-1} integrated luminosity respectively are shown in Fig. 6c and d. In Fig. 7 we show the bounds obtained using the integrated cross section with the lower bound of integration, $p_{T\min}$, optimized to maximize the sensitivity using the same integrated luminosities as above. For comparison with other analysis, we give in Table 1 the 95% C.L. limits varying one parameter at a time. We caution the reader that these numbers can be misleading as cancellations between the different anomalous couplings can conspire to give a prediction in apparent agreement with the Standard Model.

At HERA the process $ep \to \gamma\nu X$ will improve the present limit on $\delta\kappa_\gamma$ obtained from the measurement of associated γW production by the UA2 experiment at the CERN $\bar{p}p$ collider where it was found $-3.5 < \kappa_\gamma < 5.9$ and $-3.6 < \lambda_\gamma < 3.5$ at 95% C.L. [29]. The limits obtained from the Tevatron are unsettled at present, with two theory analysis finding significantly different limits

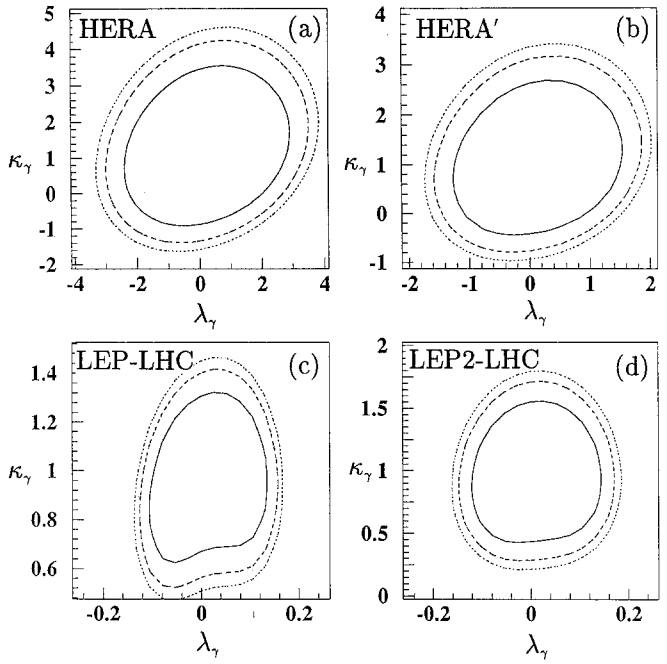

Fig. 6a–d. Confidence level contours for consistency with the Standard Model as a function of κ_γ and λ_γ based on binning the $p_{T\gamma}$ distribution into 3 bins with the binning described in the text. The solid line represents the 68% C.L. contours, the dashed line the 90% C.L. contours, and the dotted lines the 95% C.L. contours. **a** HERA for $L=1000\ \text{pb}^{-1}$. **b** HERA' for $L=1000\ \text{pb}^{-1}$. **c** LEP-LHC for $L=5000\ \text{pb}^{-1}$ and **d** LEP2-LHC for $L=500\ \text{pb}^{-1}$

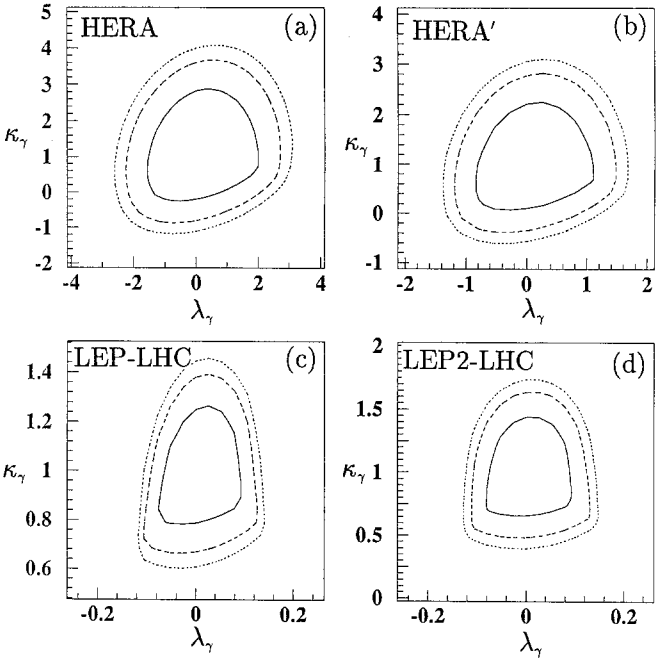

Fig. 7a–d. Confidence level contours for consistency with the Standard Model as a function of κ_γ and λ_γ based on the integrated $p_{T\gamma}$ distribution with $p_{T\gamma}(\text{min})$, the lower limit integration, chosen to optimize the sensitivity to deviations from the Standard Model. The line labelling is the same as in Fig. 6. **a** HERA for $L=1000\ \text{pb}^{-1}$. **b** HERA' for $L=1000\ \text{pb}^{-1}$. **c** LEP-LHC for $L=5000\ \text{pb}^{-1}$ and **d** LEP2-LHC for $L=500\ \text{pb}^{-1}$

Table 1. 95% confidence limit bounds on κ_γ and λ_γ found by varying one parameter at a time. The rows labelled $p_{T\text{min}}$ are based on the integrated cross section with the lower bound of integration chosen to maximize the statistical significance of deviations as described in the text and the rows labelled binning are based on the $p_{T\gamma}$ distributions with the binnings and integrated luminosities described in the text

Collider		$\delta\kappa_\gamma$	$\delta\lambda_\gamma$
HERA	$p_{T\text{min}}$	$+2.9$ -2.0	$+3.0$ -2.5
	binning	$+3.4$ -2.5	$+3.5$ -3.2
HERA'	$p_{T\text{min}}$	$+1.9$ -1.4	$+1.5$ -1.3
	binning	$+2.3$ -1.8	$+1.9$ -1.6
LEP-LHC	$p_{T\text{min}}$	$+0.42$ -0.38	$+0.13$ -0.10
	binning	$+0.43$ -0.46	$+0.16$ -0.12
LEP2-LHC	$p_{T\text{min}}$	$+0.70$ -0.58	$+0.13$ -0.12
	binning	$+0.76$ -0.76	$+0.17$ -0.15

[11, 12]. If we take the most optimistic limits, HERA would offer an improvement over the Tevatron result on $|\delta\kappa_\gamma|\simeq 3$ at 68% C.L. but not for λ_γ with $|\delta\lambda_\gamma|\simeq 1.2$ at 68% C.L. [12]. The limits that are expected at an upgraded Tevatron with $L=100\ \text{pb}^{-1}$ of $|\delta\kappa_\gamma|\simeq 1.4$ and $|\delta\lambda_\gamma|\simeq 0.47$ at 90% C.L. [12] would be better than the HERA limits from the process $ep\to\nu\gamma X$. Moreover $ep\to\nu\gamma X$ is significantly less sensitive to anomalous couplings as the process $ep\to eWX$ where $|\delta\kappa_\gamma|=0.5$ and $|\delta\lambda_\gamma|=1.2$ at 90% C.L. [15]. This reflects the fact that although $\sigma(ep\to\gamma\nu X)$, with the cuts we used, is larger than the $\sigma(ep\to eWX)$ cross section, the cross section is dominated by uninteresting bremstrahlung photons while the contributions we are interested in come from the high $p_{T\gamma}$, low cross section region of the $p_{T\gamma}$ distribution. The situation at the hypothetical HERA' collider offers some improvement, with the sensitivity to κ_γ roughly comparable to the upgraded Tevatron, but the sensitivity to λ_γ is still much less than can be achieved at the upgraded Tevatron.

At the LEP-LHC ep collider the measurement of high p_T photons turns out to be roughly as sensitive to deviations in κ_γ as can be achieved in $e^+e^-\to W^+W^-$ at LEP200 where $|\delta\kappa_\gamma|\simeq 0.3$ but is more sensitive to deviations in λ_γ than the LEP200 expectations of $|\delta\lambda_\gamma|\simeq 0.4$ [6–9]. However, associated γW production at the SSC or LHC is more sensitive to anomalous couplings. At the SSC the sensitivities are $|\delta\kappa_\gamma|\simeq 0.26$ and $|\delta\lambda_\gamma|\simeq 0.04$ at 99.99% C.L. [30, 31]. Comparing to competing processes at LEP-LHC we find that $ep\to\nu\gamma X$ is of comparable sensitivity to κ_γ as the process $ep\to\nu WX$ where $|\delta\kappa_\gamma|\simeq 0.3$ [16] but at least twice as sensitive to λ_γ where $|\delta\lambda_\gamma|\simeq 0.3$ [16]. Finally, $ep\to\nu\gamma X$ is of roughly comparable sensitivity to deviations in κ_γ and λ_γ as the process $ep\to eWX$ at LEP-LHC where $|\delta\kappa_\gamma|\simeq 0.2$ and $|\delta\lambda_\gamma|\simeq 0.1$ at 90% C.L. [15]. Although the LEP2-LHC collider has higher center

of mass energy, because it is expected to have lower luminosity, the sensitivity to anomalous couplings will be less than at a LEP-LHC ep collider.

4 Conclusions

We have examined the sensitivity of the process $ep\to\gamma\nu X$ to anomalous $WW\gamma$ couplings. We found that although at the HERA ep collider $ep\to\nu\gamma X$ offers an improvement over existing direct measurements by the UA2 and CDF $\bar{p}p$ experiments, it is less sensitive than the competing process at HERA; $ep\to eWX$. At best it would offer an independent consistency check of measurements derived from other processes. In contrast, it appears that high p_T photon production at a LEP-LHC ep collider will offer one of the more precise measurements of the $WW\gamma$ vertex for processes considered thus far.

Note added. After the original submission of this paper the author received a paper on the same subject by T. Helbig and H. Spiesberger [32]. The cross sections and distributions of the two papers are in agreement. However the sensitivities of $\Delta\kappa$ and λ differ slightly in the two papers. We attribute this to the different approaches used to measure the sensitivity to anomalous couplings.

Note added in proof: After resubmission another paper was received on the same subject by Baur and Doucheski [33] whose results agree with those of this paper.

Acknowledgements. The author is most grateful to H. Spiesberger and T. Helbig for very helpful communications, G. Couture for a useful suggestion and J. Hewett for important advice. The author also thanks Gary Levman for helpful conversations and Rahul Sinha, Paul Weber and Warren Schappert for assistance in preparing the figures. The author acknowledges the University of Guelph for the use of their Numerically Intensive Computing facility, the University of Toronto ZEUS and CDF collaborations for the use of their computers, and the Physics departments at the University of Toronto and University of Winnipeg for their hospitality where some of this work was done. This work was funded by the Natural Sciences and Engineering Research Council of Canada.

Appendix: the helicity amplitudes

In this Appendix, we outline the use of the CALKUL spinor technique and write down the helicity amplitudes for the process $ep\to\nu\gamma X$. We do not go into great detail and refer the interested reader to the literature and references therein [25]. We limit our discussion to massless fermions and massless external gauge bosons which apply to our problem. The propagators for the fermions and gauge bosons have the same form as in the trace technique so we will not discuss them here.

The spinor technique reduces strings of spinors and gamma matrices to sandwiches of spinors which can be evaluated easily. In doing so, one makes extensive use of the *left* and *right* projection operators defined by $\omega_\pm=\frac{1}{2}(1\pm\gamma_5)$. One defines two four-vectors, k_0^μ and k_1^μ, which obey the following relations:

$$k_0\cdot k_0=0,\quad k_1\cdot k_1=-1,\quad k_0\cdot k_1=0,$$

and basic spinors as:

$$u_-(k_0)\bar{u}_-(k_0)=\omega_-\not{k}_0,$$

and

$$u_+(k_0)=\not{k}_1 u_-(k_0).$$

Note that in the massless limit, one can use u and $\bar{u}$ to describe both particles and antiparticles, with the spin sum $\sum_\lambda u_\lambda(p)\bar{u}_\lambda(p)=\not{p}$. These two spinors are the building blocks for any spinor of lightlike momentum p:

$$u_\lambda(p)=\frac{\not{p}u_{-\lambda}(k_0)}{\sqrt{2p\cdot k_0}}.$$

Two identities are essential for the reduction of the strings; the spin sum given above and the Chisholm identity:

$$\bar{u}_\lambda(p_1)\gamma^\mu u_\lambda(p_2)\gamma_\mu\equiv 2u_\lambda(p_2)\bar{u}_\lambda(p_1)+2u_{-\lambda}(p_1)\bar{u}_{-\lambda}(p_2),$$

where λ is ±1 and represents the helicity state. These two identities allow one to reduce strings of spinors and gamma matrices to sandwiches of spinors. Only two of the four possible sandwiches are non-zero:

$$s(p_1,p_2)\equiv\bar{u}_+(p_1)u_-(p_2)=-s(p_2,p_1),$$

and

$$t(p_1,p_2)\equiv\bar{u}_-(p_1)u_+(p_2)=s(p_2,p_1)^*.$$

Once the amplitude has been reduced to a series of factors of $s(p_i,p_j)$ and $t(p_k,p_l)$, the expressions can be evaluated by computer. A judicious choice of the four-vectors k_0^μ and k_1^μ simplifies the evaluation of the s and t terms. For our calculation we follow [25], and use

$$p_i^\mu=(p_i^0,p_i^x,p_i^y,p_i^z)$$

$$k_0^\mu=(1,1,0,0),$$

$$k_1^\mu=(0,0,1,0),$$

to obtain

$$s(p_1,p_2)=(p_1^y+ip_1^z)\frac{\sqrt{p_2^0-p_2^x}}{\sqrt{p_1^0-p_1^x}}-(p_2^y+ip_2^z)\frac{\sqrt{p_1^0-p_1^x}}{\sqrt{p_2^0-p_2^x}}.$$

These forms are ideally suited for programming. When dealing with several diagrams, one simply evaluates the amplitudes of each diagram as complex numbers and squares the sum of the amplitudes in order to obtain the $|\text{amplitude}|^2$.

To include massless gauge bosons one represents, as usual, the gauge boson by its polarization vector. Following Kleiss and Sterling we use the definition:

$$\varepsilon_\lambda^\mu\equiv\frac{1}{\sqrt{4p\cdot k}}\bar{u}_\lambda(k)\gamma^\mu u_\lambda(p),$$

where p^μ is any lightlike four-vector not collinear to k^μ or k_0^μ. The choice of p^μ acts as a choice of gauge and provides a powerful verification of gauge invariance. Indeed, it can be shown that two different choices of p^μ will lead to two expressions that will differ by a term proportional to the photon momentum. When dotted into the amplitude, this extra term must vanish identically because of gauge invariance. Hence, two different choices of p^μ must give exactly the same answer. If they don't, there is a mistake in the amplitude. Generally, we choose p^μ to be one of the four-vectors of the problem at hand.

Using this technique we obtain for the helicity amplitudes corresponding to the Feynman diagrams of Fig. 2,

with $M_\lambda^i = \tilde{M}_\lambda^i/(4p_\gamma \cdot k)^{1/2}$,

$$\begin{aligned}
\tilde{M}_L^a &= \tfrac{1}{2} ieg^2 D_W(p_u - p_d) D_W(p_e - p_\nu) \\
&\times \{4t(p_\nu, p_d) s(p_u, p_e)[t(p_\gamma, p_u) s(p_u, k) \\
&- t(p_\gamma, p_d) s(p_d, k)] - 2[(1+\kappa) + \tilde{\lambda}(p_e - p_\nu)^2] \\
&\times t(p_\gamma, p_d) s(p_u, k) t(p_\nu, p_\gamma) s(p_\gamma, p_e) \\
&+ 2[(1+\kappa) + \tilde{\lambda}(p_u - p_d)^2] \\
&\times t(p_\gamma, p_\nu) s(p_e, k)[t(p_d, p_e) s(p_e, p_u) - t(p_d, p_\nu) s(p_\nu, p_u)] \\
&- \tilde{\lambda}[t(p_\gamma, p_u) s(p_u, k) - t(p_\gamma, p_d) s(p_d, k)] \\
&\times [t(p_d, p_e) s(p_e, p_u) - t(p_d, p_\nu) s(p_\nu, p_u)] t(p_\nu, p_\gamma) s(p_\gamma, p_e) \\
&+ \tilde{\lambda}[t(p_\gamma, p_e) s(p_e, k) - t(p_\gamma, p_\nu) s(p_\nu, k)] \\
&\times [t(p_\nu, p_u) s(p_u, p_e) - t(p_\nu, p_d) s(p_d, p_e)] t(p_d, p_\gamma) s(p_\gamma, p_u)\},
\end{aligned}$$

$$\begin{aligned}
\tilde{M}_R^a &= \tfrac{1}{2} ieg^2 D_W(p_u - p_d) D_W(p_e - p_\nu) \\
&\times \{4t(p_\nu, p_d) s(p_u, p_e)[s(p_\gamma, p_u) t(p_u, k) \\
&- s(p_\gamma, p_d) t(p_d, k)] - 2[(1+\kappa) + \tilde{\lambda}(p_e - p_\nu)^2] s(p_\gamma, p_u) \\
&\times t(p_d, k) t(p_\nu, p_\gamma) s(p_\gamma, p_e) + 2[(1+\kappa) + \tilde{\lambda}(p_u - p_d)^2] \\
&\times s(p_\gamma, p_e) t(p_\nu, k)[t(p_d, p_e) s(p_e, p_u) - t(p_d, p_\nu) s(p_\nu, p_u)] \\
&- \tilde{\lambda}[s(p_\gamma, p_u) t(p_u, k) - s(p_\gamma, p_d) t(p_d, k)] \\
&\times [t(p_d, p_e) s(p_e, p_u) - t(p_d, p_\nu) s(p_\nu, p_u)] t(p_\nu, p_\gamma) s(p_\gamma, p_e) \\
&+ \tilde{\lambda}[s(p_\gamma, p_e) t(p_e, k) - s(p_\gamma, p_\nu) t(p_\nu, k)] \\
&\times [t(p_\nu, p_u) s(p_u, p_e) - t(p_\nu, p_d) s(p_d, p_e)] t(p_d, p_\gamma) s(p_\gamma, p_u)\},
\end{aligned}$$

$$\begin{aligned}
\tilde{M}_L^{\bar{a}} &= \tfrac{1}{2} ieg^2 D_W(p_{\bar{d}} - p_{\bar{u}}) D_W(p_e - p_\nu) \\
&\times \{4t(p_\nu, p_{\bar{d}}) s(p_{\bar{u}}, p_e)[t(p_\gamma, p_{\bar{d}}) s(p_{\bar{d}}, k) \\
&- t(p_\gamma, p_{\bar{u}}) s(p_{\bar{u}}, k)] - 2[(1+\kappa) + \tilde{\lambda}(p_e - p_\nu)^2] \\
&\times t(p_\gamma, p_{\bar{d}}) s(p_{\bar{u}}, k) t(p_\nu, p_\gamma) s(p_\gamma, p_e) + 2[(1+\kappa) \\
&+ \tilde{\lambda}(p_{\bar{d}} - p_{\bar{u}})^2] t(p_\gamma, p_\nu) s(p_e, k)[t(p_{\bar{d}}, p_e) s(p_e, p_{\bar{u}}) \\
&- t(p_{\bar{d}}, p_\nu) s(p_\nu, p_{\bar{u}})] - \tilde{\lambda}[t(p_\gamma, p_{\bar{d}}) s(p_{\bar{d}}, k) \\
&- t(p_\gamma, p_{\bar{u}}) s(p_{\bar{u}}, k)][t(p_{\bar{d}}, p_e) s(p_e, p_{\bar{u}}) \\
&- t(p_{\bar{d}}, p_\nu) s(p_\nu, p_{\bar{u}})] t(p_\nu, p_\gamma) s(p_\gamma, p_e) \\
&+ \tilde{\lambda}[t(p_\gamma, p_e) s(p_e, k) - t(p_\gamma, p_\nu) s(p_\nu, k)] \\
&\times [t(p_\nu, p_{\bar{d}}) s(p_{\bar{d}}, p_e) - t(p_\nu, p_{\bar{u}}) s(p_{\bar{u}}, p_e)] t(p_{\bar{d}}, p_\gamma) s(p_\gamma, p_{\bar{u}})\},
\end{aligned}$$

$$\begin{aligned}
\tilde{M}_R^{\bar{a}} &= \tfrac{1}{2} ieg^2 D_W(p_{\bar{d}} - p_{\bar{u}}) D_W(p_e - p_\nu) \\
&\times \{4t(p_\nu, p_{\bar{d}}) s(p_{\bar{u}}, p_e)[s(p_\gamma, p_{\bar{d}}) t(p_{\bar{d}}, k) \\
&- s(p_\gamma, p_{\bar{u}}) t(p_{\bar{u}}, k)] - 2[(1+\kappa) + \tilde{\lambda}(p_e - p_\nu)^2] \\
&\times s(p_\gamma, p_{\bar{u}}) t(p_{\bar{d}}, k) t(p_\nu, p_\gamma) s(p_\gamma, p_e) \\
&+ 2[(1+\kappa) + \tilde{\lambda}(p_{\bar{d}} - p_{\bar{u}})^2] \\
&\times s(p_\gamma, p_e) t(p_\nu, k)[t(p_{\bar{d}}, p_e) s(p_e, p_{\bar{u}}) - t(p_{\bar{d}}, p_\nu) s(p_\nu, p_{\bar{u}})] \\
&- \tilde{\lambda}[s(p_\gamma, p_{\bar{d}}) t(p_{\bar{d}}, k) - s(p_\gamma, p_{\bar{u}}) t(p_{\bar{u}}, k)] \\
&\times [t(p_{\bar{d}}, p_e) s(p_e, p_{\bar{u}}) - t(p_{\bar{d}}, p_\nu) s(p_\nu, p_{\bar{u}})] t(p_\nu, p_\gamma) s(p_\gamma, p_e) \\
&+ \tilde{\lambda}[s(p_\gamma, p_e) t(p_e, k) - s(p_\gamma, p_\nu) t(p_\nu, k)] \\
&\times [t(p_\nu, p_{\bar{d}}) s(p_{\bar{d}}, p_e) - t(p_\nu, p_{\bar{u}}) s(p_{\bar{u}}, p_e)] \\
&\times t(p_{\bar{d}}, p_\gamma) s(p_\gamma, p_{\bar{u}})\},
\end{aligned}$$

$$\begin{aligned}
\tilde{M}_L^b &= -2ieg^2 D(p_e - p_\gamma) D_W(p_u - p_d) \\
&\times t(p_\nu, p_d) s(p_u, p_e) t(p_e, p_\gamma) s(k, p_e), \\
\tilde{M}_R^b &= -2ieg^2 D(p_e - p_\gamma) D_W(p_u - p_d) \\
&\times t(p_\nu, p_d)[s(p_u, p_e) t(p_e, k) - s(p_u, p_\gamma) t(p_\gamma, k)] s(p_\gamma, p_e), \\
\tilde{M}_L^{\bar{b}} &= -2ieg^2 D(p_e - p_\gamma) D_W(p_{\bar{d}} - p_{\bar{u}}) \\
&\times t(p_\nu, p_{\bar{d}}) s(p_{\bar{u}}, p_e) t(p_e, p_\gamma) s(k, p_e), \\
\tilde{M}_R^{\bar{b}} &= -2ieg^2 D(p_e - p_\gamma) D_W(p_{\bar{d}} - p_{\bar{u}}) \\
&\times t(p_\nu, p_{\bar{d}})[s(p_{\bar{u}}, p_e) t(p_e, k) - s(p_{\bar{u}}, p_\gamma) t(p_\gamma, k)] s(p_\gamma, p_e), \\
\tilde{M}_L^c &= 2iQ_u eg^2 D(p_u - p_\gamma) D_W(p_e - p_\nu) \\
&\times t(p_d, p_\nu) s(p_e, p_u) t(p_u, p_\gamma) s(k, p_u), \\
\tilde{M}_R^c &= 2iQ_u eg^2 D(p_u - p_\gamma) D_W(p_e - p_\nu) \\
&\times t(p_d, p_\nu)[s(p_e, p_u) t(p_u, k) - s(p_e, p_\gamma) t(p_\gamma, k)] s(p_\gamma, p_u), \\
\tilde{M}_L^{\bar{c}} &= -2iQ_d eg^2 D(p_{\bar{d}} - p_\gamma) D_W(p_e - p_\nu) \\
&\times t(p_{\bar{d}}, p_\gamma)[s(k, p_{\bar{d}}) t(p_{\bar{d}}, p_\nu) - s(k, p_\gamma) t(p_\gamma, p_\nu)] s(p_e, p_{\bar{u}}), \\
\tilde{M}_R^{\bar{c}} &= -2iQ_d eg^2 D(p_{\bar{d}} - p_\gamma) D_W(p_e - p_\nu) \\
&\times t(p_{\bar{d}}, k) s(p_\gamma, p_{\bar{d}}) t(p_{\bar{d}}, p_\nu) s(p_e, p_{\bar{u}}), \\
\tilde{M}_L^d &= 2iQ_d eg^2 D(p_d + p_\gamma) D_W(p_e - p_\nu) \\
&\times t(p_d, p_\gamma)[s(k, p_d) t(p_d, p_\nu) + s(k, p_\gamma) t(p_\gamma, p_\nu)] s(p_e, p_u), \\
\tilde{M}_R^d &= 2iQ_d eg^2 D(p_d + p_\gamma) D_W(p_e - p_\nu) \\
&\times t(p_d, k) s(p_\gamma, p_d) t(p_d, p_\nu) s(p_e, p_u), \\
\tilde{M}_L^{\bar{d}} &= -2iQ_u eg^2 D(p_{\bar{u}} + p_\gamma) D_W(p_e - p_\nu) \\
&\times t(p_{\bar{d}}, p_\nu) s(p_e, p_{\bar{u}}) t(p_{\bar{u}}, p_\gamma) s(k, p_{\bar{u}}), \\
\tilde{M}_R^{\bar{d}} &= -2iQ_u eg^2 D(p_{\bar{u}} + p_\gamma) D_W(p_e - p_\nu) \\
&\times t(p_{\bar{d}}, p_\nu)[s(p_e, p_{\bar{u}}) t(p_{\bar{u}}, k) + s(p_e, p_\gamma) t(p_\gamma, k)] s(p_\gamma, p_{\bar{u}}),
\end{aligned}$$

where the propagator factors are defined by $D(p) = p^{-2}$ and $D_W(p) = (p^2 - M_W^2)^{-1}$ and $Q_u = +\frac{2}{3}$ and $Q_d = -\frac{1}{3}$. The subscript refers to the helicity of the photon. The four-momenta p_e, p_u, p_d, p_ν, p_γ, $p_{\bar{d}}$, and $p_{\bar{u}}$ are defined in Fig. 2.

References

1. S.L. Glashow: Nucl. Phys. 22 (1961) 579; S. Weinberg: Phys. Rev. Lett. 19 (1967) 1264; A. Salam: Proc. of the 8th Nobel Symposium, N. Svartholm. (ed.) New York: Willey 1968
2. C. Jarlskog: Proceedings of the XXV Conference on High Energy Physics, Singapore, 1990. Singapore: World Scientific 1991
3. B. Campbell: Beyond the Standard Model?, Proceedings of the Lake Louise Institute 1990 p. 138, A. Astbury et. al., (eds.) Singapore: World Scientific 1990
4. U. Amaldi et. al.: Phys. Rev. D36 (1987) 1385; G. Costa et. al.: Nucl. Phys. B297 (1988) 244; P. Langacker, M. Luo, A.K. Mann: Rev. Mod. Phys. 64 (1992) 87
5. F. Dydak: Proceedings of the XXV Conference on High Energy Physics, Singapore, 1990. Singapore: World Scientific 1991
6. K. Hagiwara et. al.: Nucl. Phys. B282 (1987) 253
7. D. Zeppenfeld: Phys. Lett. 183B (1987) 380
8. D. Treille et. al.: Proceedings of the ECFA Workshop on LEP 200 vol. 2, p. 414, A. Böhm, W. Hoogland, (eds.), Aachen (1986), CERN 87-08
9. G. Kane, J. Vidal, C.P. Yuan: Phys. Rev. D39 (1989) 2617

10. J. Cortez, K. Hagiwara, F. Herzog: Nucl. Phys. B278 (1986) 26
11. M. Samuel et. al.: Phys. Rev. Let. 67 (1991) 9; M. Samuel et. al.: Phys. Rev. D44 (1991) 2064
12. U. Baur, E.L. Berger: Phys. Rev. D41 (1990) 1476 and references therein
13. C.H. Llewellyn–Smith, B. Wiik: DESY 77/36 (1977); P. Salati, J.C. Wallet: Z. Phys. C – Particles and Fields 16 (1982) 155; A.N. Kamal et al.: Phys. Rev. D24 (1984) 2482; H. Neufeld: Z. Phys. C – Particles and Fields 17 (1983) 145; G. Altarelli et al.: Nucl. Phys. B262 (1985) 204; E. Gabrielli: Mod. Phys. Lett. A1 (1986) 465; M. Böhm, A. Rosado: Z. Phys. C – Particles and Fields 39 (1988) 275
14. D. Atwood et al.: *W* Production in *ep* Collisions, Proceedings of the 1988 Snowmass Summer Study High Energy Physics in the 1990's, p. 264
15. U. Baur, D. Zeppenfeld: Nucl. Phys. B325 (1989) 253
16. D. Atwood et. al.: *W* Production at *ep* Colliders in the Process $ep \to W^- \nu + X$, Proceedings of the 1990 Summer Study on Research Directions for the Decade, Snowmass, Colorado, 1990, University of Wisconsin preprint MAD/PH/591 (1990)
17. H. Spiesberger: Nucl. Phys. B349 (1991) 109; D. Yu. Bardin, Č. Burdík, P.Ch. Christova, T. Riemann: Z. Phys. C – Particles and Fields 44 (1989) 149
18. D. Atwood et. al.: *ep* Collider Experiments and Physics, Proceedings of the 1990 Summer Study on Research Directions for the Decade, Snowmass, Colorado, 1990, University of Wisconsin preprint WISC-EX-90-312 (1990)
19. G. Wolf: HERA: Physics, Machine and Experiments, Proceedings of the Lake Louise Institute 1986, p. 155. Singapore: World Scientific 1986
20. J. Feltesse: Experimentation at LEP/LHC, Proceedings of the Large Hadron Collider Workshop, Aachen, Vol. I. p. 219, 1990, CERN 90-10
21. K. Gaemers, G. Gounaris: Z. Phys. C – Particles and Fields 1 (1979) 259
22. F. Boudjema, K. Hagiwara, C. Hamzaoui, K. Numata: Phys. Rev. D43 (1991) 2223
23. W.J. Marciano, A. Queijeiro: Phys. Rev. D33 (1986) 3449
24. J.M. Cornwall, D.N. Levin, G. Tiktopoulos: Phys. Rev. Lett. 30 (1973) 1268; Phys. Rev. D10 (1974) 1145; C.H. Llewellyn Smith: Phys. Lett. 46B (1973) 233; S.D. Joglekar: Ann. Phys. 83 (1974) 427
25. R. Kleiss, W.J. Stirling: Nucl. Phys. B262 (1985) 235 and references therein
26. See for example: V. Barger, R. Phillips: Collider physics. New York: Addison-Wesley 1987
27. D. Duke, J. Owens: Phys. Rev. D30 (1984) 49
28. D. H. Saxon: Development of the ZEUS Detector, Proceedings of the HERA Workshop Vol. 2 p. 903, R.D. Peccei, (ed.) Hamburg 1987
29. J. Alitti et. al.: The UA2 Collaboration, Phys. Lett. 277B (1992) 194
30. U. Baur, D. Zeppenfeld: Nucl. Phys. B308 (1988) 127
31. F. Pastore, M. Pepe: Proceedings of the Large Hadron Collider Workshop, Aachen, Vol. II, p. 106, 1990, CERN 90-10
32. T. Helbig, H. Spiesberger: Nucl. Phys. B373 (1992) 73
33. U. Baur, M.A. Doucheski: University of Madison Report MAD/PH/692 (1992)